Population genetic analysis reveals the role of natural selection and phylogeography on genome-wide diversity in an extremely compact and reduced microsporidian genome

Pascal Angst[1*], Dieter Ebert[1], and Peter D. Fields[1]

[1] Department of Environmental Sciences, Zoology, University of Basel, Basel, Switzerland

[*] Corresponding author
E-mail: pascal.angst@unibas.ch (PA)

Abstract

The determinants of variation in a species' genome-wide nucleotide diversity include historical, environmental, and stochastic aspects. This diversity can inform us about the species' past and present evolutionary dynamics. In parasites, the mode of transmission and the interactions with the host might supersede the effects of these aspects in shaping parasite genomic diversity. We used genomic samples from ten populations of the microsporidian parasite *Ordospora colligata* to investigate present genomic diversity and how it was shaped by evolutionary processes, specifically, the role of phylogeography, co-phylogeography (with the host), natural selection, and transmission mode. Although very closely related microsporidia cause diseases in humans, *O. colligata* is specific to the freshwater crustacean *Daphnia magna* and has one of the smallest known eukaryotic genomes. We found an overlapping phylogeography between *O. colligata* and its host highlighting the long-term, intimate relationship between them. The observed geographic distribution reflects previous findings that *O. colligata* exhibits adaptations to colder habitats, which differentiates it from other microsporidian gut parasites of *D. magna* predominantly found in warmer areas. The co-phylogeography allowed us to calibrate the *O. colligata* phylogeny and thus estimate its mutation rate. We found patterns of more efficient purifying selection in *O. colligata* relative to other microsporidia sharing the same host, which likely allowed this parasite to maintain its very compact genome. We also identified regions under potential selection related to coevolution including the ribosomal protein L24, a leucyl-tRNA synthetase, and a putative ABC-like lipid transport protein. Our whole-genome study provides insights into the evolution of one of the most reduced eukaryotic genomes and shows how different processes shape genomic diversity of an obligate parasite.

Author summary

Microsporidia are intracellular parasites that infect vertebrates, invertebrates, and even unicellular organisms. Due to their high variation in many aspects of life history and

genomics, microsporidia have become a model clade for understanding evolutionary processes related to intracellular parasitism. However, the evolution of extreme genomic architectures in microsporidia and the coevolution with their hosts is still under-surveyed, especially given their role in human disease. Here, we study past and present evolutionary dynamics in a microsporidian species with one of the smallest known eukaryotic genomes, *O. colligata*. Close relatives of *O. colligata* cause death and disease in humans and agriculturally important animals. We show that purifying selection helped maintaining its reduced, compact genome and corroborate hypotheses about the evolution of different genome sizes in microsporidia. Importantly, we utilize the highly resolved phylogeny of its host to estimate the parasite's mutation rate. This methodology allowed us to establish the first mutation rate estimate for a microsporidium, an estimate which is within the range of mutation rates estimated for phylogenetically related, non-parasitic fungi. Our study exemplifies how the combined knowledge about a species' biology, ecology, and genomic diversity helps to resolve its evolutionary dynamics, in particular when phylogenomic information can be brought to bear for both host and parasite.

Introduction

Understanding a species' genome-wide nucleotide diversity requires information about historical conditions (e.g., phylogeography and population structure), environmental conditions (e.g., adaptation to local climate), and stochastic processes (e.g., genetic drift and founder events) [1–3]. The contribution of each factor to the observed genomic diversity is highly variable. For example, in species prone to small population sizes, alleles may reach fixation solely due to genetic drift [4]. In contrast, in larger populations, natural selection is more efficient in preventing deleterious mutations from being fixed and in deterministically increasing the frequency of beneficial alleles. For parasites, hosts are part of the environment, with interactions between host and parasite possibly having profound impact on the parasite's genomic diversity [5]. A distinct feature of parasite life history is its mode of transmission. A parasite can be transmitted vertically (from parent to offspring), horizontally (no parent-progeny relationship between hosts) or mixed-mode (featuring

vertical and horizontal transmission) [6]. The genetic diversity of specific regions under selection, or genome-wide allele frequencies might change due to the parasite's mode of transmission [7]. Notably, the acquisition of vertical transmission by horizontally transmitted parasites was suggested to increase the potential for stochastic processes to produce random changes in the genome, because with vertical transmission population bottlenecks become more likely and thus effective population sizes, N_e, would be reduced [8]. Disentangling the effects of parasite-specific life histories from more general processes on a genomic level is still a challenge in the field of evolutionary genomics.

Microsporidia are a clade of intracellular parasites that is characterized by high variation in many aspects of life history and genomics. They cause diseases commonly referred to as microsporidiosis in agriculturally important animals, honeybees, and immunocompromised humans, among others [9,10] and are reported to infect even unicellular organisms [11]. A growing body of research features them as a model clade for understanding evolutionary processes related to extreme parasitism [10,11]. Microsporidia are phylogenetically associated with the fungi, but show high specialization to intracellular life-style combined with a large variation in life histories [12]. Most microsporidia do not have mitochondria but take up energy from their host using transmembrane transporters, although a few species have maintained mitochondria (e.g., [13]). Their genome size (about two to 50 Megabase pairs) and number of genes vary extremely [10], but microsporidia generally have a small number of genes and small genome size, including one of the smallest known eukaryotic genomes [14]. Recent work suggests that large genomes evolved in microsporidia due to the accumulation of repetitive elements when the strength of purifying selection decreases [15]. For example, large, gene-sparse genomes evolved in the microsporidian genera *Hamiltosporidium* and *Nosema* after a switch from horizontal transmission to mixed-mode transmission, which reduced N_e [8]. However, only ~18 % of the species are potentially vertically transmitted [11], while the more common exclusive horizontal transmission should allow for large N_e and the maintenance of the typical streamlined, i.e., reduced and compact, genomes.

110 Hosts of several microsporidia are planktonic freshwater crustacea of the genus *Daphnia*,
111 well-established model systems in ecology, evolution, and in the study of host-parasite
112 interactions [16–18]. Several microsporidia that infect *D. magna* have been studied both
113 ecologically, as well as on the genomic level, which is important when ecological scenarios
114 are used to explain genome evolution. Examples include the microsporidium
115 *Hamiltosporidium tvaerminnensis*, a microsporidium with a large genome size and mixed-
116 mode of transmission [19–22], and several microsporidian gut parasites – e.g. *Glugoides*
117 *intestinalis*, *Mitosporidium daphniae*, and *Ordospora colligata* – that have small genomes,
118 look superficially similar under the microscope, infect the same host tissue, and are of
119 relatively low virulence to the host [13,23,24]. However, the three mentioned *D. magna* gut
120 microsporidia diverge substantially on the molecular level [25]. *O. colligata* has received a
121 lot of attention because it has one of the most reduced genomes across all eukaryotes and
122 is closely related to the microsporidian genus *Encephalitozoon* that primarily infects humans
123 and other mammals [14]. This species features in several ecological and evolutionary studies
124 (e.g., [26–29]), some of which suggest the species is adapted to colder habitats [30].
125 Compared to, for example, *H. tvaerminnensis*, *O. colligata* is suggested to exhibit large
126 population sizes that may be a key factor for maintaining its streamlined genome [8].
127 Importantly, *O. colligata* is transmitted entirely horizontally [31], and little is known about
128 the evolution of exclusively horizontally transmitted microsporidian parasites.
129
130 In this population genomic study, we characterize genomic diversity across the species
131 range of *O. colligata*. We aimed to understand the relative contribution of phylogeography,
132 selection, and mode of transmission to shaping the variation in nucleotide diversity. The
133 phylogeography of *D. magna*, the only known host of *O. colligata*, shows three main
134 lineages and isolation-by-distance (IBD) [32–35]. Based on neutral assumptions, we
135 expected a shared phylogeography between host and obligate parasite, i.e., co-
136 cladogenesis. Furthermore, because of *O. colligata*'s horizontal mode of transmission and its
137 streamlined genome, we expected to find a constant, large population size, allowing for
138 efficient selection. We wanted to use sequentially Markovian coalescent analyses and
139 McDonald-Kreitman tests to estimate the species' effective population size history and rate
140 of adaptive evolution, respectively. We expected to find a higher selection efficacy in *O.*

141 *colligata* than previously published in *Hamiltosporidium*, which would support the
142 hypothesis by Haag et al. [8] that the mode of transmission is a driving factor for the
143 evolution of genome size in microsporidia. Specifically, horizontal transmission is expected
144 to go hand in hand with large N_e and the maintenance of a streamlined genome [8]. At least
145 in part, our population genomic study corroborates earlier speculation about mechanisms
146 driving the evolution of strongly diverged genome sizes in microsporidia by investigating the
147 relative importance and interplay of biologically meaningful processes shaping the variation
148 in genomic diversity.
149

150 Results

151

152 Samples, mapping, and sequence variation

153 The accuracy of microscopy in identifying *D. magna* microsporidian gut parasites on a
154 species level was not as high as we had assumed. By using the combination of microscopy
155 and PCR, we could reliably identify species, and we found that *D. magna* shows infections
156 with microsporidian gut parasites across its Holarctic species range (Fig 1, S1 Table). *O.*
157 *colligata* showed the widest geographic distribution but was absent from southern regions.
158 Genomic samples of ten sequenced host clones sufficiently represented the *O. colligata*
159 genome to describe its variation in genomic diversity (Table 1). The percentage of
160 sequencing reads, originating from the combined sequencing of host and parasite, being
161 mapped to the parasite's genome ranged from 0.22 to 2.97 % for *O. colligata*. The average
162 whole-genome coverage for *O. colligata* was greater than 10× in all samples. *O. colligata* has
163 a SNP density of approximately five SNPs per Kbp and a total number of 12,427 SNPs. The
164 average whole-genome estimate of π based on one Kbp windows was 0.003, approximately
165 half a percent.
166 The *O. colligata* genome has at least three regions that were horizontally
167 transmitted from the host [14]. Windows overlapping with these regions showed increased
168 diversity due to unintentional mapping of *D. magna* reads (Fig 2). Other windows within the
169 99th percentiles for π overlapped with functionally annotated genes (locus IDs as adopted
170 from Pombert et al. [14]: the ribosomal protein L24 (M896_051540), a leucyl-tRNA

171 synthetase (M896_060290) and a putative ABC-like lipid transport protein (M896_121220)),
172 of which a putative ABC-like lipid transport protein additionally had the fourth highest π_N/π_S
173 ratio, i.e., it might experience strong positive or balancing selection (S2 Table). The
174 remaining windows within the 99th percentiles for π did not overlap with annotated genes.
175

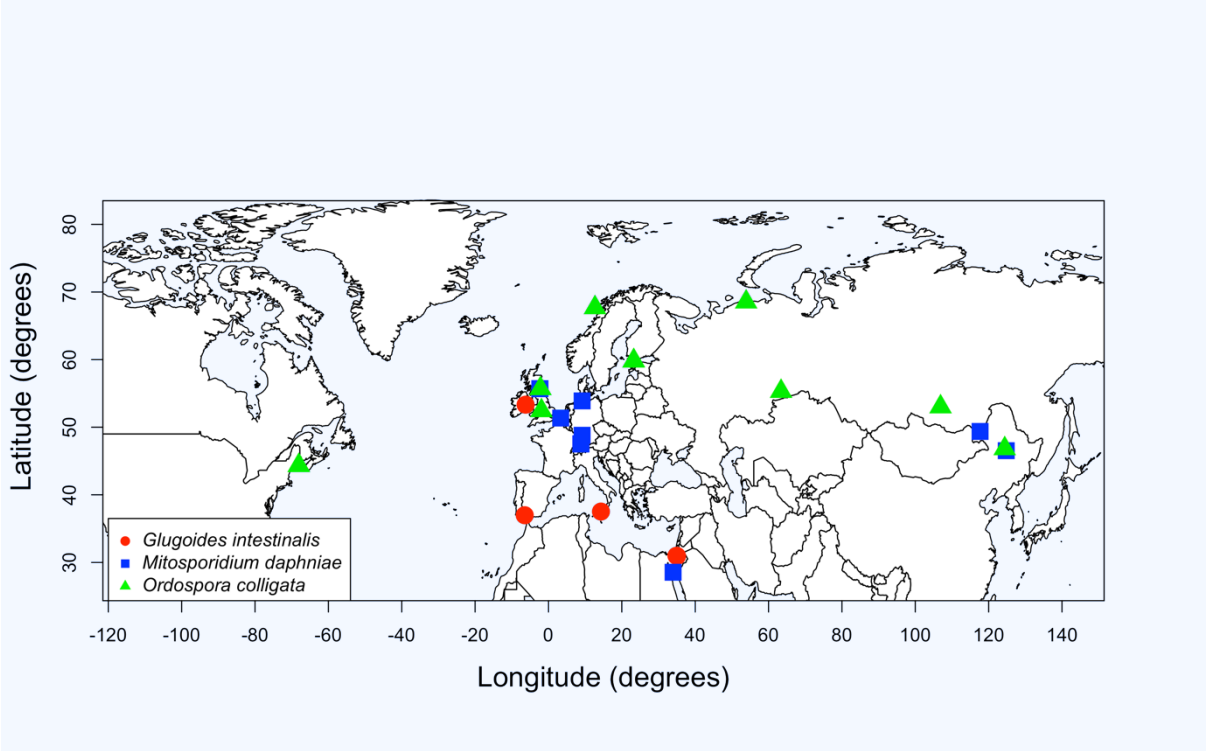

176
177 **Fig 1. Sampling distribution of three *D. magna* gut microsporidia.** Based on sampling within
178 the framework of the *D. magna* diversity panel, we found wide-range distributions of the
179 host species-specific microsporidia *Glugoides intestinalis* (red circles), *Mitosporidium*
180 *daphniae* (blue squares), and *Ordospora colligata* (green triangles). *O. colligata* has the
181 widest distribution within the Holarctic host-distribution, while the other two microsporidia
182 have not been observed in Northern America.
183
184 **Table 1. Sample information.**

Sample ID	Country	Latitude	Longitude	Coverage
CN-WON-2	China	46.825017	124.378953	10×
FI-SK-17-1	Finland	59.8312191	23.2577045	19×
FI-SKW-2-1	Finland	59.8329692	23.2562571	26×
GB-EP-1	Great Britain	52.4535830	-1.9194440	71×

NO-V-7	Norway	67.68696	12.67197	70×
RU-BAYA1-1	Russia	53.017833	106.886833	29×
RU-KU1-2	Russia	55.303833	63.405333	21×
US-SP131-1	United States	44.3332	-68.0632	40×
US-SP15-1	United States	44.3331	-68.0629	55×
US-SP163-1	United States	44.3336	-68.0636	37×

O. colligata's average whole-genome coverage is denoted in the last column.

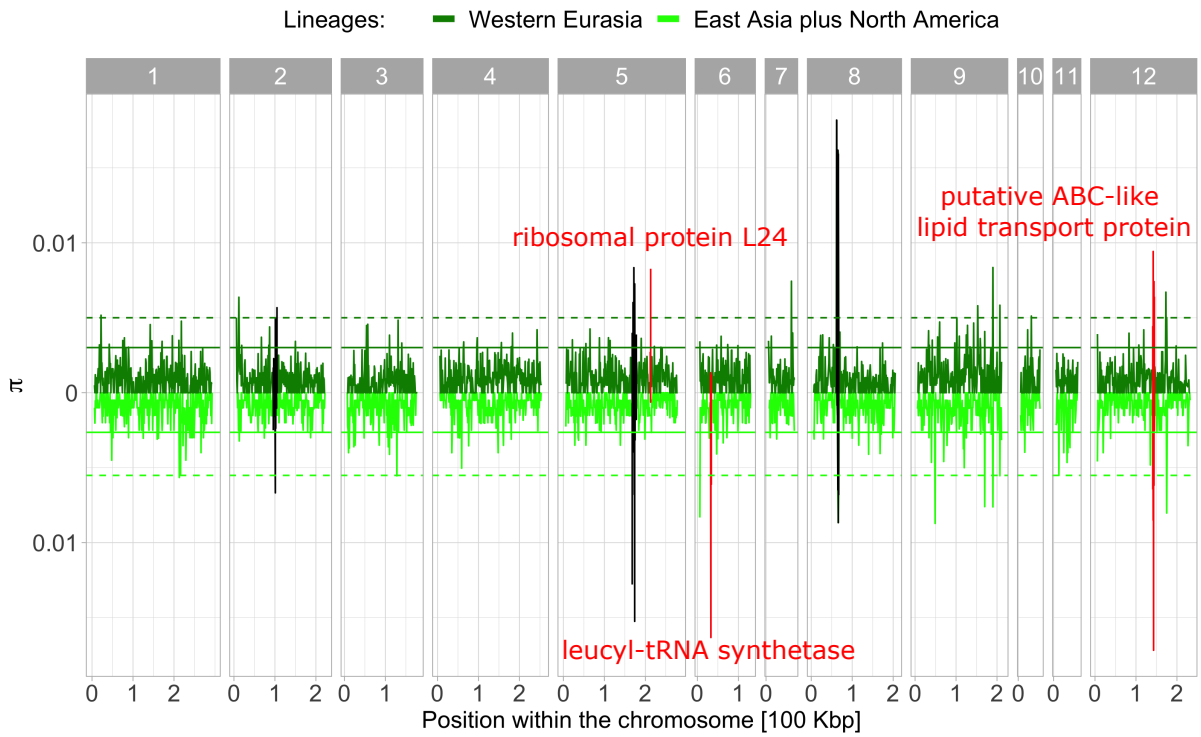

Fig 2. Average per-site nucleotide differences (π) in *O. colligata*. Per-site π is averaged over 1 Kbp windows along the genome. The π values of both main *O. colligata* lineages are presented in 12 facets corresponding to the parasite's 12 chromosomes. We used the combined sample of East Asian and North American samples to have equal sample sizes for comparing lineages (N = 5). The 95th and 99th percentiles of each lineage are indicated with a solid and a dashed line, respectively. The first and last five Kbp per chromosome were masked for better presentation. Black windows indicate increased diversity due to host-to-parasite horizontal gene transfer. Annotated genes with increased π values mentioned in the discussion are indicated in red with their locus IDs: the ribosomal protein L24 (M896_051540), a leucyl-tRNA synthetase (M896_060290) and a putative ABC-like lipid transport protein (M896_121220).

199

200 ## Ploidy

201 Allele frequency signatures of *O. colligata* samples showed haploid characteristics in 7 out of
202 9 samples (Fig 3, S1 and S2 Figs). The other two were not as clear due to low levels of
203 polymorphisms or potential multiple infections of *O. colligata*. Specifically, no prominent
204 peaks were found in the putative allele frequency histogram calculated using ploidyNGS.
205 One peak can be seen in the k-mer histogram around the average whole-genome coverage.
206 Therefore, the trimmed sequencing reads supported a single variant for most positions
207 along the genome and no signs of heterozygosity were visible, hence *O. colligata* was
208 treated as haploid in all analyses.

209

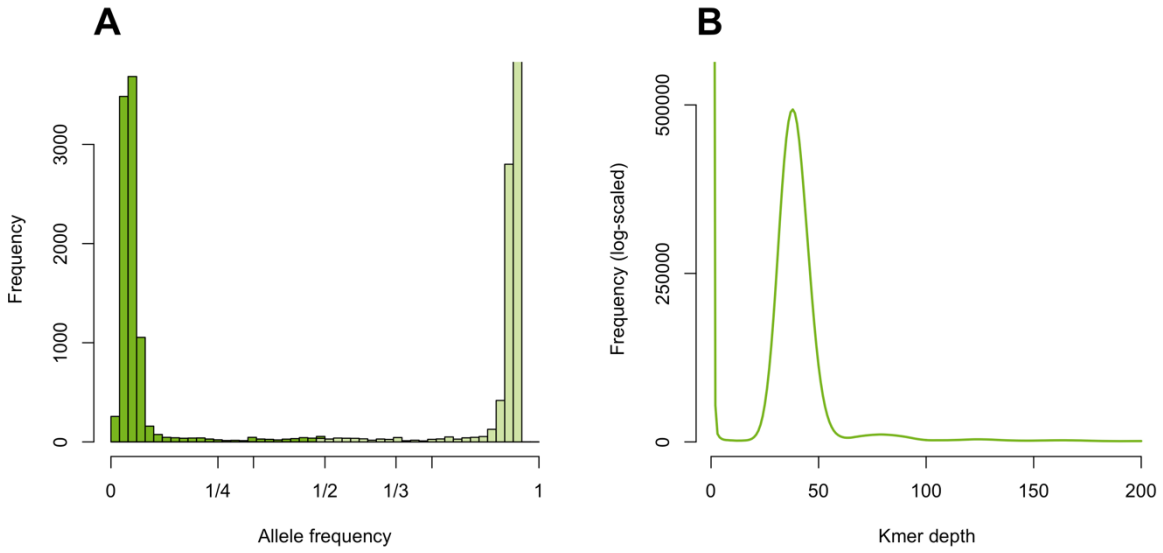

210

211 **Fig 3. Graphical summaries of the two approaches to determine ploidy levels for *O.***
212 ***colligata* sample US-SP15-1.** Histogram of allele frequency of putative alleles in the BAM file
213 found using ploidyNGS (A), where reads supported a single variant for most positions. Few
214 sites and no sharp central peak at intermediate allele frequencies is seen as would be the
215 case in diploids. Dark and light shadings of green indicate reference and alternative allele,
216 respectively. K-mer frequency histogram inferred using kmercountexact.sh (B), with a single
217 peak for homozygous sites and no secondary peaks which would indicate di-/polyploidy.

218

Population structure

To determine the shared or differing amounts of genomic variation between *O. colligata* samples, we used PCA on the whole-genome SNP data. PC1 separated samples in three clusters, which became even clearer in combination with PC2 (S3 Fig). The two PCs explained a substantial amount of genomic variation, with 63.60 % and 15.43 %, respectively. The three clusters (Western Eurasian (N = 5), East Asian (N = 2), and North American (N = 3) cluster, named according to the geographic regions the samples in each cluster originate from) were also found in the cluster analysis and the Bayesian phylogenetic tree estimation based on four-fold degenerate sites (Fig 4, S4 and S5 Figs). Pairwise relatedness in *O. colligata* was negatively correlated with geographic distance (Fig 5; R^2 = 0.54, p = 0.001), suggesting IBD.

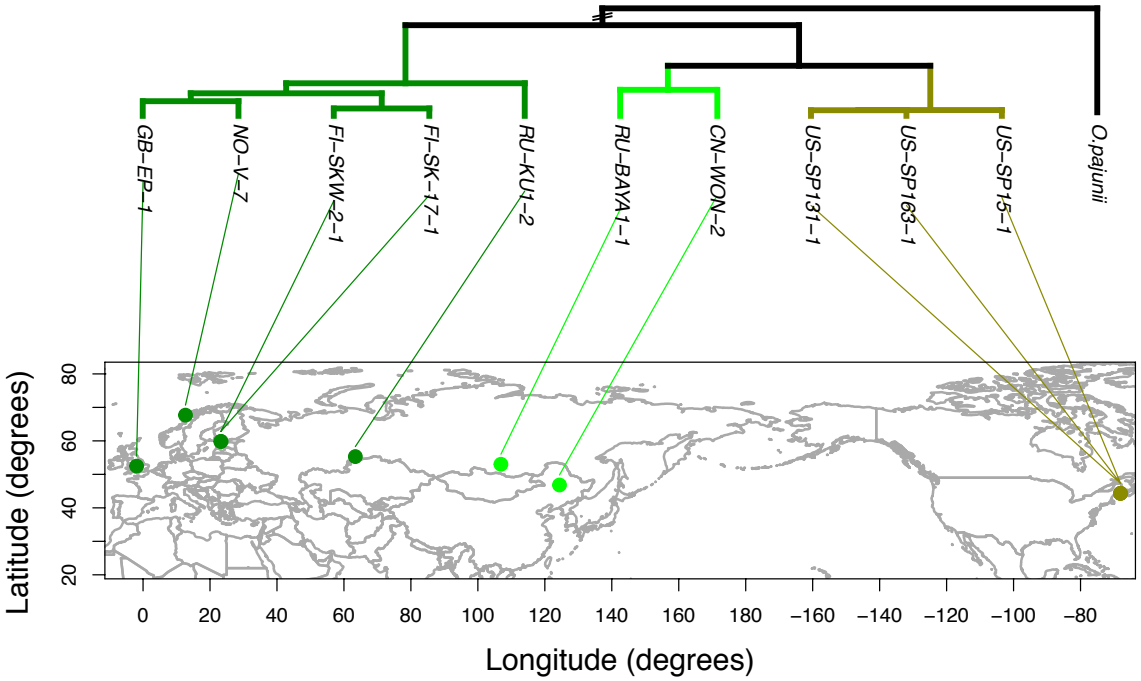

Fig 4. Geophylogeny of *O. colligata*. The tree is based on four-fold degenerate sites of single copy orthologs when compared to the outgroup, *O. pajunii*. Tree tips are connected to the sampling locality by colored lines, whereby colors indicate the main lineages inferred from population structure analyses: Western Eurasian (dark green), East Asian (lime), and North

American (olive). See S5 Fig for the correct branch length to *O. pajunii,* as it is out of scale here for better presentation.

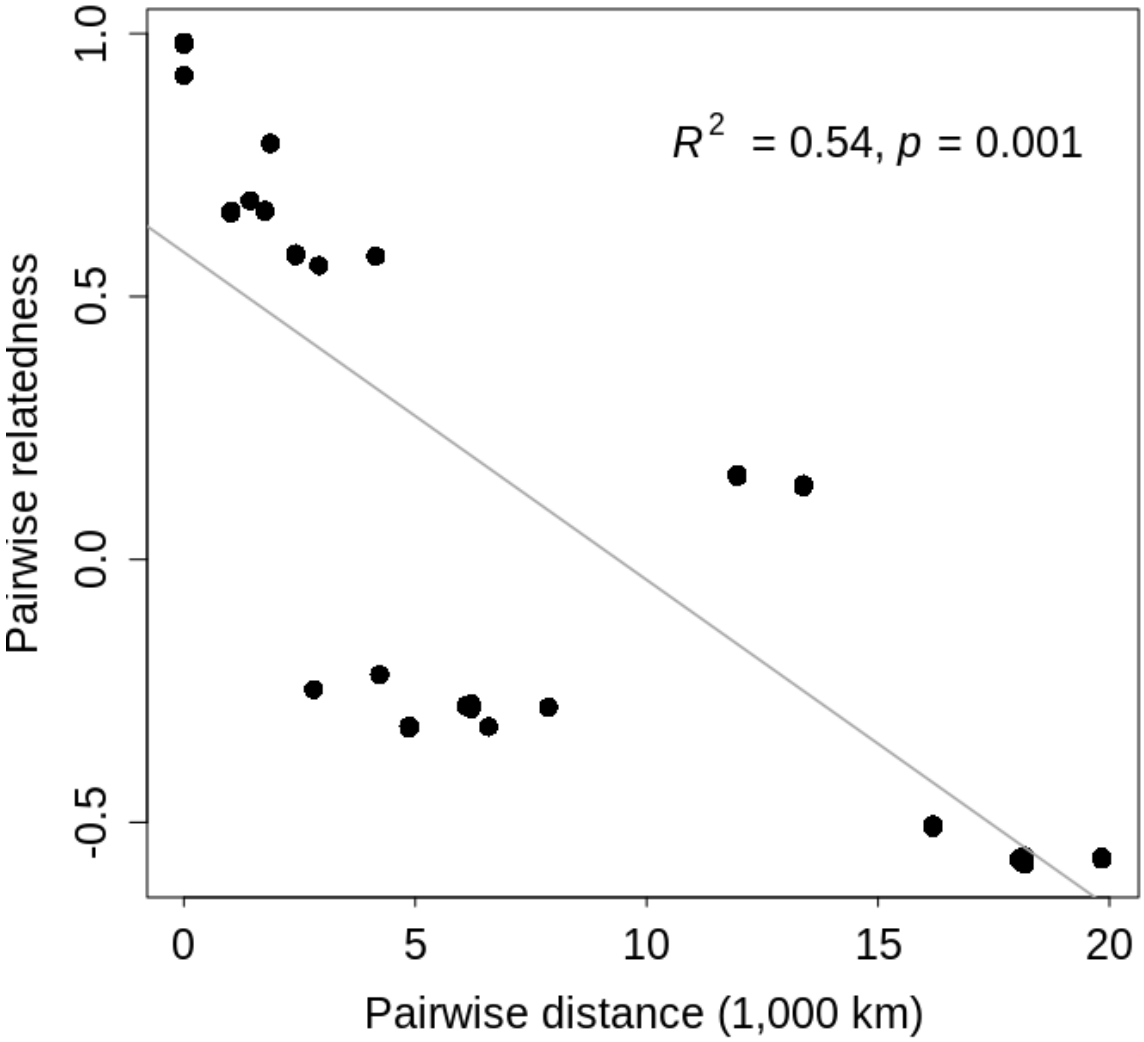

Fig 5. Isolation by distance (IBD). Pairwise relatedness is positively correlated with geographic distance. Each point represents the comparison between two samples. Statistics derive from dbMEM analysis by RDA. The grey line is a regression line based on a linear model.

Mutation rate estimation

After observing the same population structure in *O. colligata* as previously found in its only host, *D. magna*, we calibrated the molecular clock in the phylogenetic analysis using the fossil-calibrated divergence time between Western Eurasian and East Asian (plus North American) host samples [36]. We found a median divergence time between *O. colligata* Western Eurasian and East Asian (plus North American) lineages of 1.61 Mya (95 % HPD interval: 0.62-4.19 Mya), which is largely overlapping with the host divergence time estimate (1.3-9.3 Mya) [36]. The median clock rate estimate was 1.04×10^{-9} per site per year (95 % HPD interval: 2.33×10^{-10}-2.07×10^{-9} per site per year). Given published generation times of microsporidia (i.e., 63 h) [37] this would correspond to a mutation rate of 7.48×10^{-12} per site per generation (95 % HPD interval: 1.68×10^{-12}-1.49×10^{-11} per site per generation). However, given its Northern distribution, *O. colligata*, like its host, endures the long winters as resting stage (spore) without reproducing. Assuming a resting time of three to six months, its mutation rate might be between 9.98×10^{-12} and 1.50×10^{-11} per site per generation (2.24×10^{-12}-2.98×10^{-11}). These values are comparable with what has previously been reported for fungi (see e.g., [38–40]).

Efficient purifying selection

We assessed the efficacy of selection in *O. colligata* to test hypotheses about the evolution of the wide range of genome sizes observed in microsporidia. Therefore, we compared the ratio of nonsynonymous to synonymous polymorphisms, π_N/π_S, between BUSCO and non-BUSCO genes. The former are conserved genes among most microsporidia and are therefore expected to be under purifying selection. Indeed, BUSCO genes had a 1.5 times lower median π_N/π_S ratio (0.085) than non-BUSCO genes (0.130). These values are close to an estimate for BUSCO genes in the large genome sized microsporidium *H. tvaerminnensis* (0.102). However, in *H. tvaerminnensis,* non-BUSCO genes have a three times higher median π_N/π_S ratio (0.306), which is significantly different from all other (non-)BUSCO gene values mentioned here (Kruskal-Wallis $\chi^2(3) = 309.83$, $p < 0.001$). This suggests that *H. tvaerminnensis* experiences relaxed purifying selection. By implication, this means that there is relatively efficient purifying selection in *O. colligata*, likely due to its entirely vertical transmission and the consequently high N_e.

Discussion

The study of population genetics aims to understand temporal and spatial variation in genetic diversity, ideally within a framework of the ecology of the focal species. For parasites, this includes host–parasite interactions and the mode of transmission. Here, we take advantage of a model system in host-parasite evolutionary ecology, the planktonic freshwater species *Daphnia magna*, to explain genomic diversity, genome architecture, and population structure of one of its specific parasites, the microsporidium *O. colligata*. *O. colligata* is a parasite known for its small, compact genome, one of the smallest among all eukaryotic life [14]. Its host, *D. magna*, shows a clear split in its Holarctic distribution into a Western Eurasian and an East Asian (plus North American) lineage, the latter of which is subsequently divided into East Asian and North American lineages [33,35,36]. We find a pattern of co-cladogenesis with overlapping phylogeography between *O. colligata* and its host, which allows us to estimate the mutation rate of a microsporidium for the first time. Furthermore, we observe IBD, providing an explanation for the relationships among populations. We show evidence for efficient genome-wide purifying selection in *O. colligata*, which supports the hypothesis that horizontally transmitted microsporidia were able to evolve and maintain small, streamlined genomes due to high effective population sizes [8].

Host-parasite co-phylogeography

The close interaction of the intracellular microsporidia and their hosts might shape the phylogeography of the parasites to be congruent to their host's phylogeography — the within-species equivalent of the Fahrenholz rule [41], which states that host and parasite phylogenies show a pattern of co-cladogenesis. A strict co-phylogeography is expected if the parasite species' mode of transmission is uniquely vertical [42], consistent with the expectation of co-dispersal as the mechanism of parasite spread [43]. Previous attempts by Pelin et al. [44] and Angst et al. [19] to reconstruct a co-phylogeography based on whole-genome data for two microsporidian species, *N. ceranae* and *H. tvaerminnensis*, respectively, remained unsuccessful, possibly due to high (human-driven) migration or non-

306 simultaneous host-parasite expansions. In contrast, the phylogeography of *O. colligata* is
307 congruent with the host's phylogeography suggesting a long-term association and co-
308 dispersal with the host. Specifically, both host and parasite phylogenies consisted of the
309 same three geographically distinct lineages; the first lineage encompasses Western Eurasian
310 samples, the second East Asian and the third Northern American samples. Furthermore, in
311 contrast to the previously mentioned microsporidia (*N. ceranae* and *H. tvaerminnensis*), we
312 found a pattern of species-wide IBD in *O. colligata*. IBD has also been described for the host,
313 as well as for a bacterial parasite of *D. magna*, *Pasteuria ramosa* [32,35]. This pattern
314 further strengthens the assumption of co-dispersal throughout the history of *O. colligata*
315 and *D. magna*.

316 We have so far not detected *O. colligata* in southern regions. Diagnostic sequencing
317 revealed that parasite samples from the Middle East, which have been identified as *O.*
318 *colligata* using light microscopy [22], are other species, with very similar morphology and
319 pathology (Fig 1). However, given the growing evidence that *O. colligata* shows an
320 adaptation to colder habitats, it was not surprising to not find it in southern regions [30]. In
321 contrast to *O. colligata*, we confirmed the presence of the *D. magna* specific microsporidia
322 *Glugoides intestinalis* and *Mitosporidium daphniae* in Southern Europe using microscopy
323 and PCR (Fig 1). Based on our results, future research should be careful relying on
324 microscopy only for species identification, as we observed several cases of misidentification
325 of microsporidia infecting *D. magna*.

326 By calibrating the phylogenetic tree of *O. colligata* with the divergence time of the
327 Western Eurasian and East Asian (plus North American) host lineages, a time which has
328 previously been estimated using fossil data [36], we provide the first estimated mutation
329 rate of a microsporidium. Fungi, to which the microsporidia are phylogenetically associated,
330 have been shown to have low mutation rates (e.g., [38–40]). Our estimate for *O. colligata*
331 falls within the range of previously published mutation rate estimates of fungi. Therefore,
332 we find no evidence that intracellular microsporidia evolve more rapidly than their free-
333 living relatives, which might be expected based on the expectation that parasitism may
334 accelerate the evolutionary process [45]. However, no other approaches to estimate
335 mutation rates, for example, mutation accumulation experiments, have been performed for
336 microsporidia so far.

337

338 Genome evolution

339 The evolution of different genome sizes in microsporidia is an ongoing research area of
340 great interest [14,15,19,46]. In microsporidia, genome streamlining is associated with the
341 abandonment of entire metabolic pathways and fewer transposable elements.
342 Furthermore, the maintenance of streamlined microsporidian genomes was possible due to
343 efficient purifying selection, which is only possible with large effective population sizes [8].
344 In contrast, small effective population sizes, for example, in species that exhibit population
345 bottlenecks during vertical transmission, increase the power of stochastic processes and
346 reduce selection efficacy [8,47]. Also, the proliferation of repetitive elements is less
347 constrained in species with small effective population sizes. Therefore, we wanted to
348 estimate the effective population size and the rate of adaptive substitution, α (as a measure
349 for selection efficacy) in the horizontally transmitted *O. colligata* and compare it to another
350 microsporidian parasite of *D. magna*, *H. tvaerminnensis*, which has a mixed-mode
351 transmission and a small effective population size [19]. However, PSMC expects diploid
352 samples to calculate N_e and α estimated using MKTs was unreliable since our data had too
353 few intraspecies polymorphisms as opposed to the many fixed substitutions between *O.*
354 *colligata* and the outgroup (the closest known relative *O. pajunii*). We would need more
355 diversity by adding more *O. colligata* samples to the dataset or a more closely related
356 outgroup to reliably estimate α using MKTs. However, consistent with the expectation of
357 weaker purifying selection in microsporidia of larger genome sizes and additional vertical
358 transmission, we found elevated π_N/π_S ratios in non-BUSCO genes in *H. tvaerminnensis*
359 compared to *O. colligata*. In a previous comparison between the genera *Hamiltosporidium*
360 and *Ordospora*, mixed-mode transmission and larger genome size has been shown to be
361 associated with larger d_N/d_S ratios [8]. We extend the evidential basis with our between-
362 species comparison of population samples.
363

364 Describing genomic variation

365 We estimated genomic variation of the species-specific parasite *O. colligata* with samples
366 covering a large part of the host's geographic distribution. The whole-genome SNP density

367 in *O. colligata* is slightly lower than what was found for its close relative *Encephalitozoon*
368 *cuniculi* [48], which was, in contrast to the samples used in this study, isolated from
369 different host species. The low SNP density in *O. colligata* made certain analyses unreliable,
370 i.e., inferring historical N_e and MKTs. The analyses to determine ploidy levels suggest that *O.*
371 *colligata* is haploid (we did not conduct cytological analyses). However, two samples were
372 somewhat ambiguous with regard to the haploid pattern (S1 and S2 Figs), but this was in
373 part due to the quantity of segregating polymorphisms or the potential presence of multiple
374 infections of *O. colligata* in the same sample. Our methods to infer the ploidy level of *O.*
375 *colligata* would fail, however, if *O. colligata* is di- or polyploid with extremely low levels of
376 heterozygosity, an unlikely genomic characteristic.
377
378 While low levels of genomic diversity might constrain some population genetic analyses,
379 other important signals might be clearer. For example, because much of the *O. colligata*
380 genome is depauperate in SNP diversity, regions with an increased SNP density stand out
381 from the larger genomic context (Fig 2). Some of these distinctly diverse regions have
382 increased diversity due to host-to-parasite horizontal gene transfer, which Pombert et al.
383 [14] previously described (chromosomes 2, 5, and 8). Specifically, the observed excess
384 diversity may arise as the result of the unintentional mapping of *D. magna* reads to these
385 transferred regions; thus, both the host and parasite variants are conflated. More relevant
386 to the present study is how other outlier regions might be affected differently by evolution.
387 Indeed, some genes with functions relevant to the evolution of microsporidia-specific traits
388 show high sequence variation, e.g., the ribosomal protein L24 (M896_051540), a leucyl-
389 tRNA synthetase (M896_060290), and a putative ABC-like lipid transport protein
390 (M896_121220). The ribosomal protein L24 has been reported by Liu et al. [49] to be
391 differentially expressed before and after the germination of spores of the microsporidium
392 *Nosema bombycis*, suggesting its importance for the regulation of transcriptional and
393 translation activities during the infection process. Like other protein synthetases, Melnikov
394 et al. [50] reported that the leucyl-tRNA synthetase has degenerated in the microsporidium
395 *Vavraia culicis*. Malfunctioning synthetases are hypothesized to produce more diverse
396 proteomes in microsporidia than expected. ABC-like lipid transport proteins are important
397 in parasitic protists, like microsporidia, for their role in nutrient salvage [51]. While most

398 ABC transporters are outward exporters, some are described as importers in parasitic
399 protists. These importers might contribute to the parasite's nutrient uptake when living
400 inside the host cell. Moreover, the putative ABC-like lipid transport protein M896_121220
401 has the fourth highest π_N/π_S ratio, which is an indicator for positive selection, especially
402 recognizable when compared directly to the genomic background. Among the proteins with
403 high π_N/π_S ratios (S2 Table), many are annotated as hypothetical proteins. The inability to
404 annotate these genes based on sequence similarity may already be a sign of 1) their fast-
405 evolving nature and 2) their specific function in the context of coevolution between *D.*
406 *magna* and *O. colligata*.
407

408 # Conclusion

409 The existence of extreme genomic architectures in microsporidia has been known for a
410 while. To understand such large-scale genomic differences, knowledge about the different
411 species' biology is indispensable. Previously intractable problems in intracellular parasites'
412 past and present evolutionary dynamics can now be studied using genomic diversity at a
413 fine scale. Furthermore, investigating the evolution of different genome sizes in
414 microsporidia is facilitated by comparing parasites evolving in the same host, where the host
415 factor can be assumed to be similar. Therefore, this study profits from comparisons
416 between two genera of microsporidia, *Hamiltosporidium* and *Ordospora*, which share the
417 host, *D. magna*. The genomes of these microsporidian genera are affected differently by
418 coevolution with the same host. Mainly, we think that the acquisition of vertical
419 transmission in *Hamiltosporidium* led to the expansion of its genome. Contrarily, in the
420 vertically transmitted *Ordospora*, large effective population size and efficient purifying
421 selection helped maintaining its compact genome. This study adds to the growing research
422 of microsporidia supporting the observation that the mode of transmission plays an
423 important role in the evolution of genome size. This hypothesis would benefit from larger
424 comparative studies based on whole genome data across the clade of the microsporidia.
425

426 # Material and Methods

427 ## Daphnia magna Diversity Panel

428 We used parasites derived from material collected within the framework of a large-scale
429 biogeographic study of the host species, *D. magna* [34,35,52,53]. From each population,
430 animals were brought to the laboratory and one iso-female line, i.e., clone, was created. We
431 checked these clones for infections with microsporidia by phase-contrast microscopy, using
432 squash-preparations or samples of the gut. The panel includes whole-genome sequencing
433 (WGS) of *D. magna* clones with Illumina paired-end reads using HiSeq 2500 and NovaSeq
434 6000 sequencers.
435

436 ## Samples

437 Whole-genome sequences of ten *O. colligata* samples, each from a different *D. magna* clone
438 collected from a different population, were obtained from the Illumina sequencing (Table
439 1). Sequences from clones FI-SK-17-1, NO-V-7, and GB-EP-1 were reused from Haag et al. [8]
440 (NCBI database; SRA accession: SRP211974, Bioproject ID: PRJNA419750), sequences from
441 clone RU-BAYA1-1 were reused from Angst et al. [19] (NCBI database; SRA accession:
442 SRP346323, Bioproject ID: PRJNA780787), and for clone FI-SK-17-1 additional sequencing
443 was done. We used the *D. longispina*-specific *Ordospora pajunii* for analyses that needed an
444 outgroup (NCBI database; Bioproject ID: PRJNA630072 [54]). Some samples with observed
445 microsporidia gut infection (i.e., based on published criteria for identifying *O. colligata*
446 infection) showed less than 1× average whole-genome coverage for *O. colligata*. To verify
447 the presumed parasite at species level, we performed polymerase chain reactions (PCRs) of
448 the small subunit of microsporidian ribosomal DNA followed by Sanger sequencing (S1
449 Table). For this, we treated one animal per *D. magna* clone with three antibiotics
450 (streptomycin, tetracycline, ampicillin) at a concentration of 50 mg/L each for 24 h to reduce
451 non-focal DNA. To aid gut evacuation, we fed animals after 0 h and 12 h with dextran beads
452 (Sephadex 'Small' by Sigma Aldrich: 50 mm diameter) at a concentration of 0.5 g/100 mL
453 [55]. Afterward, we moved individuals into separate wells of an unskirted 96-well PCR plate
454 (Eppendorf) and removed excess fluid with a sterile pipette. Subsequently, we crushed
455 individuals using a customized rack of metallic pestles. To each well, we added 20 µL

456 microLYSIS-Plus DNA release buffer (Microzone, West Sussex, UK) and used the
457 manufacturer's tough cell lysis protocol (65 °C for 15 min; 96 °C for 2 min; 65 °C for 4 min;
458 96 °C for 1 min; 65 °C for 1 min; 96 °C for 30 s) for incubation in an Eppendorf Mastercycler
459 Nexus. Following this DNA extraction, we diluted the products to 0.1 × with deionized water
460 and set up the PCR reactions. Each 50 µL PCR took place in an Eppendorf Mastercycler
461 Nexus, with each reaction consisting of 29.5 µL deionized water, 10 µL of the diluted
462 sample, 5 µL 10 × PCR buffer, 2 µL forward and reverse primer, 1 µL dNTPs and 0.5 µL Taq
463 DNA polymerase. We used universal primers targeting the small subunit of microsporidian
464 ribosomal DNA (V1f: 5'-CACCAGGTTGATTCTGCCTGAC-3'; 1342r: 5'-
465 ACGGGCGGTGTGTACAAAGAACAG-3') [56]. The PCR conditions were 95 °C for 15 min,
466 followed by 40 cycles of 95 °C for 30 s, 67.5 °C for 90 s, and 72 °C for 90 s, and then 72 °C for
467 7 min. PCR products were sequenced by Microsynth (Balgach, Switzerland) using the Sanger
468 method on ABI 3730/3730xl machines (Applied Biosystems; Thermo Fisher Scientific). We
469 compared the obtained sequence data to the NIH genetic sequence database (GenBank)
470 [57] with the Basic Local Alignment Search Tool for nucleotides (BLASTN) on the NCBI
471 website (https://blast.ncbi.nlm.nih.gov/). The success of the DNA extraction was verified
472 before submission with an additional PCR using a *D. magna*-specific pair of primers and the
473 same PCR conditions, i.e., positive control on PCR conditions. Samples with a microscopically
474 detected microsporidian infection and a positive *D. magna* control but without a PCR
475 product for the microsporidian universal marker were assigned to infection with *M.*
476 *daphniae*, another gut microsporidium [13] which is phenotypically very similar to *O.*
477 *colligata*, but for which the primers would not be capable of generating an amplicon
478 because it is a very basal microsporidium.
479

480 Mapping and variant calling

481 We assessed raw sequencing reads for quality using FastQC v.0.11.7
482 (http://www.bioinformatics.babraham.ac.uk/projects/fastqc) and subsequently trimmed
483 them to remove low-quality sequences and adapter contamination using Trimmomatic
484 v.0.38 [58]. Unless otherwise stated, we used default parameters for bioinformatics
485 programs. We assayed successful trimming using a second run of FastQC. We downloaded
486 the genome of *O. colligata* (NCBI database; Assembly name: ASM80326v; GenBank

487 assembly accession: GCA_000803265.1, Bioproject accession: PRJNA210314 [14]) from NCBI
488 and used it as a reference for mapping quality-trimmed reads with BWA MEM v.0.7.17 [59],
489 using default parameters. We converted SAM files to BAM files, coordinate-sorted individual
490 BAM files, and removed unmapped reads using SAMtools v.1.9 [60]. Afterward, we added
491 read groups and marked duplicates for individual BAM files using Picard Toolkit v.2.18.16
492 [61]. To compute the average read depth, we used SAMtools function depth, and for variant
493 calling, we used GATK v.3.8 HaplotypeCaller in the haploid mode [62,63]. Specifically, we
494 first generated GVCFs for individual BAM files and used the GATK function GenotypeGVCF to
495 combine GVCFs into an all-site VCF. We filtered this VCF file to include only SNP variants
496 (i.e., exclude INDEL variants) using VCFtools v.0.1.16 [64].
497

498 Ploidy

499 We applied two different methods to infer the ploidy of *O. colligata* samples. First, we used
500 ploidyNGS v.3.1.2 [65] to visualize frequencies of putative alleles directly from individual
501 BAM files. Second, we output reads which mapped to the reference genome to FASTQ files
502 using BEDtools v.2.27.1 [66] and subsequently used Kmercountexact.sh, a bash script
503 included in BBMap v.38.22 [67] to generate k-mer frequency histograms. Based on the
504 results of this ploidy assessment, which were consistent across the two methodologies, *O.*
505 *colligata* was treated as haploid in all analyses requiring ploidy assignment.
506

507 Coding sequences - single-copy orthologs

508 Phylogenetic analyses and tests for selection (especially its efficacy) mostly rely on protein-
509 coding regions. To characterize variation in nucleotide diversity within the protein-coding
510 sections of the *O. colligata* samples, we needed to extract subsets of the genome-wide VCF
511 using the following approaches. Protein sequences of *O. colligata* (OC4; GenBank accession:
512 JOKQ00000000.1) were downloaded from NCBI and complemented with those of the
513 outgroup, *O. pajunii* (GenBank accession: JACCJH000000000.1 [54]). To find one-to-one
514 orthologs between the species, we used protein datasets of the two as input for OrthoMCL
515 v.2.0.9 [68]). Specifically, we followed the automated pipeline described at the following
516 Github repository: https://github.com/apetkau/orthomcl-pipeline. We aligned the identified

517 orthologous sequences of *O. colligata* and *O. pajunii* with PRANK v.170427 [69] using a
518 custom script adapted from [52]. After an initial survey of pairwise alignment quality, we
519 implemented a masking step, wherein excessively divergent or poorly aligned sequences
520 (divergence > 0.5 %) were excluded from downstream analysis. We used the R package
521 *seqinR* v.3.4-5 [70] for importing FASTA alignments and *PopGenome* v.2.7.1 [71] for the
522 manipulation of the VCF file in the next step. To produce multiple sequence alignments, we
523 generated one alternative reference for each *O. colligata* sample using the GATK-functions
524 SelectVariants and FastaAlternateReferenceMaker. We cut out coding sequences of interest
525 from the alternative references with the script gff2fasta.pl
526 (https://github.com/ISUgenomics/common_scripts). To align the resultant coding
527 sequences of the *O. colligata* ingroup samples to the *O. colligata–O. pajunii* alignments, we
528 used MAFFT v.7.407 [72,73] and its --add option. Next, we masked all positions previously
529 masked in the two species reference alignments in the multiple sequence-alignments using
530 generate_masked_ranges.py (https://gist.github.com/danielecook) and BEDtools function
531 maskfasta.
532

533 ## Sequence variation and population genetic analyses

534 We calculated the SNP density of *O. colligata* by dividing the genome lengths by the number
535 of SNPs across the full genome using VCFtools. For calculating per-site nucleotide
536 differences (π) along the *O. colligata* genome, we used pixy v.0.95 [74]. Beforehand, we
537 filtered out alleles with less than half or more than double the average sample coverage.
538 Finally, we averaged the estimated π-values over one Kilobase pair (Kbp) windows. Similarly,
539 we calculated the non-/synonymous per-site nucleotide differences (π_N and π_S) for the
540 coding sequences of *O. colligata* using the script selectionStats.py
541 (https://github.com/tatumdmortimer/popgen-stats). Both methods are consistent with
542 theoretical expectations and comparable amongst species as they take invariant sites into
543 account for their calculations [74]. The ratio of π_N and π_S was separately calculated for
544 BUSCO genes (Benchmarking Universal Single-Copy Orthologs) identified using BUSCO
545 v.4.0.1 [75] and its microsporidia_odb10 database (Creation date: 2020-08-05) and
546 compared to published π_N/π_S values of *H. tvaerminnensis* [19].
547

548 ## Population structure and phylogenetic analyses

549 To assess population structure in *O. colligata*, we used the R v.3.5.1 [76] packages *SNPRelate*
550 v.1.14.0 and *gdsfmt* v.1.16.0 [77] for principal component analysis (PCA) as well as cluster
551 analysis with the whole-genome polymorphism data. Additionally, to test for IBD, we
552 compared the samples' pairwise relatedness with their pairwise geographic distance.
553 Therefore, we used the R package *hierfstat* v.0.5-7 [78] to calculate the pairwise relatedness
554 and *geodist* v.0.0.3 [79] to calculate the geographic distance between samples with the
555 geodesic measure. We measured the distance to the North American samples across the
556 Bering Strait to account for the likely dispersal route of host and parasite given their
557 population structure. For file import and format conversions we used *VCFR* and *adegenet*
558 v.2.1.2 [80] in R. We tested for association between relatedness and geographic distance
559 using dbMEM analysis by RDA. Specifically, we transformed the explanatory variable,
560 geographic distance, into dbMEMs using the *adespatial* v.0.3-14 [81] R package and
561 decomposed the response variable, genetic relatedness, into principal components using
562 the R base *stats* function prcomp. We then used the R package *vegan* v.2.5-7 [82] for RDA
563 and assessed significance with 1,000 permutations.

564 In addition to looking at whole-genome diversity, we also focused directly on the
565 phylogenetic signal in protein-coding regions of the genome. We concatenated previously
566 extracted single-copy ortholog gene alignments into a single sequence and filtered for four-
567 fold degenerate sites with MEGA v.7.16.0617 [83], which we used as input for Bayesian
568 phylogenetic analysis in BEAST2 v.2.6.2 [84,85]. We prepared inputs using the graphical
569 user-interface application BEAUti, which is part of BEAST2. We used the GTR+G substitution
570 model, because this was the most likely model for our data according to jModelTest v.2.1.10
571 [86], a strict clock, the Yule model as tree prior, and a MCMC chain of 10,000,000 iterations.
572 After observing a clear split between Western Eurasian and East Asian (plus North
573 American) samples, we further used a most recent common ancestor prior with a log-
574 normal distribution for this split and switched to a calibrated Yule model. Specifically, we
575 used M = 1, S = 0.775, and offset = 0.45 for the log-normal distribution which translates to a
576 median of 3.17 Mya and a 95 % CI of 1.21-10.2 Mya and reflects the likely range for this split
577 in the host [36]. We investigated the convergence of the analysis using Tracer v.1.7.1 [87]
578 and ensured that the effective sample size (ESS) of the parameters was greater than 200.

579 For generating the final tree, the posterior sample of trees was summarized to a maximum
580 clade credibility tree using TreeAnnotator, which is part of BEAST2, with the first 10 % of the
581 MCMC chain discarded as burn-in. Lastly, we visualized the obtained tree on a map of the
582 Holarctic using the R package *phytools* v.0.7-20 [88].
583

584 ## Demographic history and rate of adaptive nucleotide substitutions

585 We applied the McDonald–Kreitman test (MKT) [89] and a more recent derivate, the
586 asymptotic MKT [90], to estimate α. However, the imbalance between low intraspecific
587 diversity and high divergence to the outgroup *O. pajunii* in the multi-sequence alignments of
588 single-copy orthologs impeded reliable estimation of α (Jesús Murga-Moreno, pers. comm.).
589 We refrained from estimating past and present N_e using PSMC after determining that *O.*
590 *colligata* is likely haploid.
591

592 # Acknowledgements

593 We thank Jürgen Hottinger, Urs Stiefel, Michelle Krebs and Andrea Cabalzar for help in the
594 field and laboratory. We thank members of the Ebert group for providing feedback on the
595 study and the manuscript.
596

597 # References

598

599 1. Font-Porterias N, Caro-Consuegra R, Lucas-Sánchez M, Lopez M, Giménez A, Carballo-
600 Mesa A, et al. The Counteracting Effects of Demography on Functional Genomic
601 Variation: The Roma Paradigm. Molecular Biology and Evolution. 2021 Jul
602 1;38(7):2804–17.

603 2. Horníková M, Marková S, Lanier HC, Searle JB, Kotlík P. A dynamic history of admixture
604 from Mediterranean and Carpathian glacial refugia drives genomic diversity in the
605 bank vole. Ecology and Evolution. 2021;11(12):8215–25.

606 3. Marske KA, Thomaz AT, Knowles LL. Dispersal barriers and opportunities drive multiple

607 levels of phylogeographic concordance in the Southern Alps of New Zealand.
608 Molecular Ecology. 2020;29(23):4665–79.

609 4. Leroy T, Rousselle M, Tilak M-K, Caizergues AE, Scornavacca C, Recuerda M, et al.
610 Island songbirds as windows into evolution in small populations. Current Biology. 2021
611 Mar 22;31(6):1303-1310.e4.

612 5. Ebert D, Fields PD. Host–parasite co-evolution and its genomic signature. Nature
613 Reviews Genetics. 2020 Aug 28;21:754–68.

614 6. Chrostek E, Pelz-Stelinski K, Hurst GDD, Hughes GL. Horizontal Transmission of
615 Intracellular Insect Symbionts via Plants. Front Microbiol. 2017 Nov 28;8:2237.

616 7. Russell SL, Pepper-Tunick E, Svedberg J, Byrne A, Castillo JR, Vollmers C, et al.
617 Horizontal transmission and recombination maintain forever young bacterial symbiont
618 genomes. PLOS Genetics. 2020 Aug 25;16(8):e1008935.

619 8. Haag KL, Pombert J-F, Sun Y, de Albuquerque NRM, Batliner B, Fields P, et al.
620 Microsporidia with Vertical Transmission Were Likely Shaped by Nonadaptive
621 Processes. Lynch M, editor. Genome Biology and Evolution. 2020 Jan 1;12(1):3599–
622 614.

623 9. Buczek K, Trytek M, Deryło K, Borsuk G, Rybicka-Jasińska K, Gryko D, et al. Bioactivity
624 studies of porphyrinoids against microsporidia isolated from honeybees. Sci Rep. 2020
625 Jul 14;10(1):11553.

626 10. Wadi L, Reinke AW. Evolution of microsporidia: An extremely successful group of
627 eukaryotic intracellular parasites. PLOS Pathogens. 2020 Feb 13;16(2):e1008276.

628 11. Murareanu BM, Sukhdeo R, Qu R, Jiang J, Reinke AW. Generation of a Microsporidia
629 Species Attribute Database and Analysis of the Extensive Ecological and Phenotypic
630 Diversity of Microsporidia. mBio. 2021;12(3):e01490-21.

631 12. Corradi N. Microsporidia: Eukaryotic Intracellular Parasites Shaped by Gene Loss and
632 Horizontal Gene Transfers. Annu Rev Microbiol. 2015 Oct 15;69(1):167–83.

633 13. Haag KL, James TY, Pombert J-F, Larsson R, Schaer TMM, Refardt D, et al. Evolution of
634 a morphological novelty occurred before genome compaction in a lineage of extreme
635 parasites. PNAS. 2014 Oct 28;111(43):15480–5.

636 14. Pombert J-F, Haag KL, Beidas S, Ebert D, Keeling PJ. The *Ordospora colligata* Genome:
637 Evolution of Extreme Reduction in Microsporidia and Host-To-Parasite Horizontal
638 Gene Transfer. mBio. 2015 Jan 13;6(1):e02400-14.

639 15. de Albuquerque NRM, Ebert D, Haag KL. Transposable element abundance correlates
640 with mode of transmission in microsporidian parasites. Mobile DNA. 2020 Jun
641 23;11:19.

642 16. Altermatt F, Ebert D. Genetic diversity of *Daphnia magna* populations enhances
643 resistance to parasites. Ecology Letters. 2008;11(9):918–28.

644 17. Ebert D. Host–parasite coevolution: Insights from the *Daphnia*–parasite model system.
645 Current Opinion in Microbiology. 2008 Jun 1;11(3):290–301.

646 18. Orlansky S, Ben-Ami F. Genetic resistance and specificity in sister taxa of *Daphnia*:
647 insights from the range of host susceptibilities. Parasites Vectors. 2019 Dec;12(1):545.

648 19. Angst P, Ebert D, Fields PD. Demographic history shapes genomic variation in an
649 intracellular parasite with a wide geographic distribution. Molecular Ecology. 0(0):1–
650 17.

651 20. Decaestecker E, Declerck S, De Meester L, Ebert D. Ecological implications of parasites
652 in natural *Daphnia* populations. Oecologia. 2005 Jul;144(3):382–90.

653 21. Ebert D, Hottinger JW, Pajunen VI. Temporal and Spatial Dynamics of Parasite Richness
654 in a *Daphnia* Metapopulation. Ecology. 2001;82(12):3417–34.

655 22. Goren L, Ben-Ami F. Ecological correlates between cladocerans and their
656 endoparasites from permanent and rain pools: patterns in community composition
657 and diversity. Hydrobiologia. 2013 Jan 1;701(1):13–23.

658 23. Larsson JIR, Ebert D, Vávra J, Voronin VN. Redescriptjon of *Pleistophora intestinalis*
659 Chatton, 1907, a microsporidian parasite of *Daphnia magna* and *Daphnia puiex*, with
660 establishment of the new genus *Glugoides* (Microspora, glugeidae). European Journal
661 of Protistology. 1996 May;32(2):251–61.

662 24. Larsson JIR, Ebert D, Vávra J. Ultrastructural study and description of *Ordospora*
663 *colligata* gen. et sp. nov. (microspora, ordosporidae fam. nov.), a new microsporidian
664 parasite of *Daphnia magna* (Crustacea, Cladocera). European Journal of Protistology.

1997 Dec 17;33(4):432–43.

25. Williams BAP, Hamilton KM, Jones MD, Bass D. Group-specific environmental sequencing reveals high levels of ecological heterogeneity across the microsporidian radiation. Environmental Microbiology Reports. 2018;10(3):328–36.

26. Ebert D, Lipsitch M, Mangin KL. The Effect of Parasites on Host Population Density and Extinction: Experimental Epidemiology with *Daphnia* and Six Microparasites. The American Naturalist. 2000 Nov 1;156(5):459–77.

27. Kirk D, Luijckx P, Stanic A, Krkošek M. Predicting the Thermal and Allometric Dependencies of Disease Transmission via the Metabolic Theory of Ecology. The American Naturalist. 2019 May 1;193(5):661–76.

28. Manzi F, Halle S, Seemann L, Ben-Ami F, Wolinska J. Sequential infection of *Daphnia magna* by a gut microsporidium followed by a haemolymph yeast decreases transmission of both parasites. Parasitology. 2021 Nov;148(13):1566–77.

29. Refardt D, Ebert D. Inference of parasite local adaptation using two different fitness components. J Evol Biol. 2007 May;20(3):921–9.

30. Kirk D, Jones N, Peacock S, Phillips J, Molnár PK, Krkošek M, et al. Empirical evidence that metabolic theory describes the temperature dependency of within-host parasite dynamics. PLOS Biology. 2018 Feb 7;16(2):e2004608.

31. Ebert D. Ecology, epidemiology, and evolution of parasitism in Daphnia. Bethesda (MD): National Library of Medicine (US), National Center for Biotechnology Information; 2005.

32. Andras JP, Fields PD, Ebert D. Spatial population genetic structure of a bacterial parasite in close coevolution with its host. Molecular Ecology. 2018;27(6):1371–84.

33. Bekker EI, Karabanov DP, Galimov YR, Haag CR, Neretina TV, Kotov AA. Phylogeography of Daphnia magna Straus (Crustacea: Cladocera) in Northern Eurasia: Evidence for a deep longitudinal split between mitochondrial lineages. PLOS ONE. 2018 Mar 15;13(3):e0194045.

34. Fields PD, Reisser C, Dukić M, Haag CR, Ebert D. Genes mirror geography in *Daphnia magna*. Molecular Ecology. 2015;24(17):4521–36.

694 35. Fields PD, Obbard DJ, McTaggart SJ, Galimov Y, Little TJ, Ebert D. Mitogenome
695 phylogeographic analysis of a planktonic crustacean. Molecular Phylogenetics and
696 Evolution. 2018 Dec 1;129:138–48.

697 36. Cornetti L, Fields PD, Van Damme K, Ebert D. A fossil-calibrated phylogenomic analysis
698 of *Daphnia* and the Daphniidae. Molecular Phylogenetics and Evolution. 2019 Aug
699 1;137:250–62.

700 37. Kramer JP. Generation time of the microsporidian *Octosporea muscaedomesticae* flu
701 in adult *Phormia regina* (Meigen) (Diptera, Calliphoridae). Z Parasitenkd. 1965 Mar
702 3;25:309–13.

703 38. Bezmenova AV, Zvyagina EA, Fedotova AV, Kasianov AS, Neretina TV, Penin AA, et al.
704 Rapid Accumulation of Mutations in Growing Mycelia of a Hypervariable Fungus
705 *Schizophyllum commune*. Molecular Biology and Evolution. 2020 Aug 1;37(8):2279–86.

706 39. Ene IV, Farrer RA, Hirakawa MP, Agwamba K, Cuomo CA, Bennett RJ. Global analysis of
707 mutations driving microevolution of a heterozygous diploid fungal pathogen. Proc Natl
708 Acad Sci U S A. 2018 Sep 11;115(37):E8688–97.

709 40. Zhu YO, Siegal ML, Hall DW, Petrov DA. Precise estimates of mutation rate and
710 spectrum in yeast. Proc Natl Acad Sci U S A. 2014 Jun 3;111(22):E2310-2318.

711 41. Fahrenholz H. Ectoparasiten und Abstammungslehre. Zoologischer Anzeiger.
712 1913;(41):371–4.

713 42. Werren JH, Baldo L, Clark ME. *Wolbachia*: master manipulators of invertebrate
714 biology. Nat Rev Microbiol. 2008 Oct;6(10):741–51.

715 43. Page RDM. Tangled Trees: Phylogeny, Cospeciation, and Coevolution. University of
716 Chicago Press; 2003. 364 p.

717 44. Pelin A, Selman M, Aris-Brosou S, Farinelli L, Corradi N. Genome analyses suggest the
718 presence of polyploidy and recent human-driven expansions in eight global
719 populations of the honeybee pathogen *Nosema ceranae*. Environ Microbiol. 2015
720 Nov;17(11):4443–58.

721 45. Moran NA. Accelerated evolution and Muller's rachet in endosymbiotic bacteria. Proc
722 Natl Acad Sci U S A. 1996 Apr 2;93(7):2873–8.

723 46. Parisot N, Pelin A, Gasc C, Polonais V, Belkorchia A, Panek J, et al. Microsporidian
724 genomes harbor a diverse array of transposable elements that demonstrate an
725 ancestry of horizontal exchange with metazoans. Genome Biol Evol. 2014 Aug
726 28;6(9):2289–300.

727 47. Lynch M. The origins of genome architecture. Sunderland (MA): Sinauer Associates.;
728 2007.

729 48. Pombert J-F, Xu J, Smith DR, Heiman D, Young S, Cuomo CA, et al. Complete Genome
730 Sequences from Three Genetically Distinct Strains Reveal High Intraspecies Genetic
731 Diversity in the Microsporidian *Encephalitozoon cuniculi*. Eukaryotic Cell. 2013 Apr
732 1;12(4):503–11.

733 49. Liu H, Chen B, Hu S, Liang X, Lu X, Shao Y. Quantitative Proteomic Analysis of
734 Germination of *Nosema bombycis* Spores under Extremely Alkaline Conditions. Front
735 Microbiol. 2016 Sep 21;7:1459.

736 50. Melnikov SV, Rivera KD, Ostapenko D, Makarenko A, Sanscrainte ND, Becnel JJ, et al.
737 Error-prone protein synthesis in parasites with the smallest eukaryotic genome. Proc
738 Natl Acad Sci U S A. 2018 Jul 3;115(27):E6245–53.

739 51. Dean P, Major P, Nakjang S, Hirt RP, Embley TM. Transport proteins of parasitic
740 protists and their role in nutrient salvage. Front Plant Sci. 2014 Apr 29;5.

741 52. Fields PD, McTaggart SJ, Reisser CMO, Haag C, Palmer WH, Little TJ, et al. Population-
742 genomic analysis identifies a low rate of global adaptive fixation in the proteins of the
743 cyclical parthenogen *Daphnia magna*. Journal of Molecular Biology and Evolution.
744 2022;msac048.

745 53. Seefeldt L, Ebert D. Temperature- versus precipitation-limitation shape local
746 temperature tolerance in a Holarctic freshwater crustacean. Proceedings of the Royal
747 Society B: Biological Sciences. 2019 Jul 24;286(1907):20190929.

748 54. de Albuquerque N, Haag K, Fields P, Cabalzar A, Ben-Ami F, Pombert J-F, et al. A new
749 microsporidian parasite, *Ordospora pajunii* sp. nov (Ordosporidae), of *Daphnia*
750 *longispina* highlights the value of genomic data for delineating species boundaries.
751 Journal of Eukaryotic Microbiology.

752 55. Dukić M, Berner D, Roesti M, Haag CR, Ebert D. A high-density genetic map reveals
753 variation in recombination rate across the genome of *Daphnia magna*. BMC Genetics.
754 2016 Oct 13;17(1):137.

755 56. Madyarova EV, Adelshin RV, Dimova MD, Axenov-Gribanov DV, Lubyaga YA, Timofeyev
756 MA. Microsporidian Parasites Found in the Hemolymph of Four Baikalian Endemic
757 Amphipods. PLOS ONE. 2015 Jun 18;10(6):e0130311.

758 57. Benson DA, Cavanaugh M, Clark K, Karsch-Mizrachi I, Lipman DJ, Ostell J, et al.
759 GenBank. Nucleic Acids Res. 2013 Jan;41(Database issue):D36-42.

760 58. Bolger AM, Lohse M, Usadel B. Trimmomatic: a flexible trimmer for Illumina sequence
761 data. Bioinformatics. 2014 Aug 1;30(15):2114–20.

762 59. Li H. Aligning sequence reads, clone sequences and assembly contigs with BWA-MEM.
763 arXiv:13033997 [q-bio]. 2013 May 26;

764 60. Li H, Handsaker B, Wysoker A, Fennell T, Ruan J, Homer N, et al. The Sequence
765 Alignment/Map format and SAMtools. Bioinformatics. 2009 Aug 15;25(16):2078–9.

766 61. Broad Institute. “Picard Toolkit.” [Internet]. Broad Institute, GitHub Repository; 2019.
767 Available from: http://broadinstitute.github.io/picard/

768 62. McKenna A, Hanna M, Banks E, Sivachenko A, Cibulskis K, Kernytsky A, et al. The
769 Genome Analysis Toolkit: A MapReduce framework for analyzing next-generation DNA
770 sequencing data. Genome Res. 2010 Jan 9;20(9):1297–303.

771 63. Van der Auwera GA, Carneiro MO, Hartl C, Poplin R, del Angel G, Levy-Moonshine A, et
772 al. From FastQ data to high confidence variant calls: the Genome Analysis Toolkit best
773 practices pipeline. Curr Protoc Bioinformatics. 2013 Oct 15;11(1110):11.10.1-11.10.33.

774 64. Danecek P, Auton A, Abecasis G, Albers CA, Banks E, DePristo MA, et al. The variant
775 call format and VCFtools. Bioinformatics. 2011 Aug 1;27(15):2156–8.

776 65. Augusto Corrêa dos Santos R, Goldman GH, Riaño-Pachón DM. ploidyNGS: visually
777 exploring ploidy with Next Generation Sequencing data. Bioinformatics. 2017 Aug
778 15;33(16):2575–6.

779 66. Quinlan AR. BEDTools: the Swiss-army tool for genome feature analysis. Current
780 protocols in bioinformatics. 2014 Sep 8;47:11.12.1-11.12.34.

781 67. Bushnell B. BBMap [Internet]. 2016. Available from:
782 https://sourceforge.net/projects/bbmap/

783 68. Li L, Stoeckert CJ, Roos DS. OrthoMCL: Identification of Ortholog Groups for Eukaryotic
784 Genomes. Genome Res. 2003 Jan 9;13(9):2178–89.

785 69. Löytynoja A. Phylogeny-aware alignment with PRANK. In: Russell DJ, editor. Multiple
786 Sequence Alignment Methods. Totowa, NJ: Humana Press; 2014. p. 155–70. (Methods
787 in Molecular Biology).

788 70. Charif D, Lobry JR. SeqinR 1.0-2: A Contributed Package to the R Project for Statistical
789 Computing Devoted to Biological Sequences Retrieval and Analysis. In: Bastolla U,
790 Porto M, Roman HE, Vendruscolo M, editors. Structural Approaches to Sequence
791 Evolution: Molecules, Networks, Populations. Berlin, Heidelberg: Springer; 2007. p.
792 207–32. (Biological and Medical Physics, Biomedical Engineering).

793 71. Pfeifer B, Wittelsbürger U, Ramos-Onsins SE, Lercher MJ. PopGenome: An Efficient
794 Swiss Army Knife for Population Genomic Analyses in R. Mol Biol Evol. 2014 Jul
795 1;31(7):1929–36.

796 72. Katoh K, Misawa K, Kuma K, Miyata T. MAFFT: a novel method for rapid multiple
797 sequence alignment based on fast Fourier transform. Nucleic Acids Res. 2002 Jul
798 15;30(14):3059–66.

799 73. Katoh K, Standley DM. MAFFT Multiple Sequence Alignment Software Version 7:
800 Improvements in Performance and Usability. Mol Biol Evol. 2013 Apr 1;30(4):772–80.

801 74. Korunes KL, Samuk K. pixy: Unbiased estimation of nucleotide diversity and divergence
802 in the presence of missing data. bioRxiv. 2020 Jun 28;2020.06.27.175091.

803 75. Seppey M, Manni M, Zdobnov EM. BUSCO: Assessing Genome Assembly and
804 Annotation Completeness. In: Kollmar M, editor. Gene Prediction: Methods and
805 Protocols. New York, NY: Springer; 2019. p. 227–45. (Methods in Molecular Biology).

806 76. R Core Team. R: The R Project for Statistical Computing [Internet]. Vienna, Austria: R
807 Foundation for Statistical Computing; 2018. Available from: https://www.r-
808 project.org/

809 77. Zheng X, Levine D, Shen J, Gogarten SM, Laurie C, Weir BS. A high-performance

810 computing toolset for relatedness and principal component analysis of SNP data.
811 Bioinformatics. 2012 Dec 1;28(24):3326–8.

812 78. Goudet J, Thibaut J. hierfstat: Estimation and Tests of Hierarchical F-Statistics. 2020.

813 79. Padgham M, Sumner MD. geodist: Fast, Dependency-Free Geodesic Distance
814 Calculations. 2019.

815 80. Jombart T. adegenet: a R package for the multivariate analysis of genetic markers.
816 Bioinformatics. 2008 Jun 1;24(11):1403–5.

817 81. Dray S, Bauman D, Blanchet G, Borcard D, Clappe S, Guenard G, et al. adespatial:
818 Multivariate Multiscale Spatial Analysis [Internet]. 2021. Available from:
819 https://CRAN.R-project.org/package=adespatial

820 82. Oksanen J, Blanchet FG, Friendly M, Kindt R, Legendre P, McGlinn D, et al. vegan:
821 Community Ecology Package [Internet]. 2020. Available from: https://CRAN.R-
822 project.org/package=vegan

823 83. Kumar S, Stecher G, Tamura K. MEGA7: Molecular Evolutionary Genetics Analysis
824 Version 7.0 for Bigger Datasets. Mol Biol Evol. 2016 Jul 1;33(7):1870–4.

825 84. Bouckaert R, Vaughan TG, Barido-Sottani J, Duchêne S, Fourment M, Gavryushkina A,
826 et al. BEAST 2.5: An advanced software platform for Bayesian evolutionary analysis.
827 Pertea M, editor. PLoS Comput Biol. 2019 Apr 8;15(4):e1006650.

828 85. Drummond AJ, Rambaut A, Shapiro B, Pybus OG. Bayesian Coalescent Inference of
829 Past Population Dynamics from Molecular Sequences. Mol Biol Evol. 2005 May
830 1;22(5):1185–92.

831 86. Darriba D, Taboada GL, Doallo R, Posada D. jModelTest 2: more models, new heuristics
832 and parallel computing. Nat Methods. 2012 Aug;9(8):772–772.

833 87. Rambaut A, Drummond AJ, Xie D, Baele G, Suchard MA. Posterior Summarization in
834 Bayesian Phylogenetics Using Tracer 1.7. Syst Biol. 2018 Sep 1;67(5):901–4.

835 88. Revell LJ. phytools: an R package for phylogenetic comparative biology (and other
836 things). Methods in Ecology and Evolution. 2012;3(2):217–23.

837 89. McDonald JH, Kreitman M. Adaptive protein evolution at the Adh locus in *Drosophila*.
838 Nature. 1991 Jun 20;351(6328):652–4.

90. Haller BC, Messer PW. asymptoticMK: A Web-Based Tool for the Asymptotic McDonald–Kreitman Test. G3: Genes, Genomes, Genetics. 2017 May 1;7(5):1569–75.

Data availability statement

Analysis scripts are available at https://github.com/pascalangst/Angst_etal_2022_PLOSPathog and raw data is deposited at the NCBI SRA database (BioProject IDs PRJNA814405).

Author contributions

All authors designed the study. DE collected the samples. PA analyzed the data and wrote the manuscript. All authors reviewed the manuscript.

Supporting information

S1 Fig. Putative allele frequency spectrum by ploidyNGS of Ordospora colligata samples. Histograms of allele frequency of putative alleles in the BAM files found using ploidyNGS, where reads supported a single variant for most positions. Dark and light shadings of colors indicate reference and alternative allele, respectively.

S2 Fig. K-mer frequency histogram of *Ordospora colligata* by kmercountexact.sh. K-mer frequency histograms inferred using kmercountexact.sh, with a single peak for homozygous sites and no secondary peaks which would indicate di-/polyploidy.

S3 Fig. PCA of genomic SNP data. PC1 vs. PC2 (A) and PC1 vs. PC3 (B).

S4 Fig. Cluster analysis of genomic SNP data.

S5 Fig. Bayesian tree inference of *Ordospora*. Node labels are posterior probabilities and the scale bar unit is average height.

S1 Table. Further microsporidian infections in the collection. Gi = *Glugoides intestinalis*, Hm = *Hamiltosporidium magnivora*, Ht = *Hamiltosporidium tvaerminnensis*, Md = *Mitosporidium daphniae*, Oc = *Ordospora colligata*. In some genomic samples, there were no sequencing reads of the parasites that were previously identified by microscopy. This led to try to identify the species with PCR using a universal marker for microsporidia. When there were spores visible under the microscope but no PCR product, the sample was tentatively assigned to be infected with *Mitosporidium daphniae*, an early diverging microsporidium, for which the microsporidian primer pair does not work.

S2 Table. List of *O. colligata* coding sequence (CDS) alignments with π_N/π_S values. The single copy orthologous protein of *O. pajunii* is denoted in the last column. Per-CDS π and π_N/π_S value were calculated using selectionstats.py. The gene annotation is derived from the original record (NCBI database; Assembly name: ASM80326v; GenBank assembly accession: GCA_000803265.1, Bioproject accession: PRJNA210314)